july 1968

the institute of electrical and electronics engineers

Proceedings of the IEEE

in this issue

INTEGRATED CIRCUIT MEMORIES

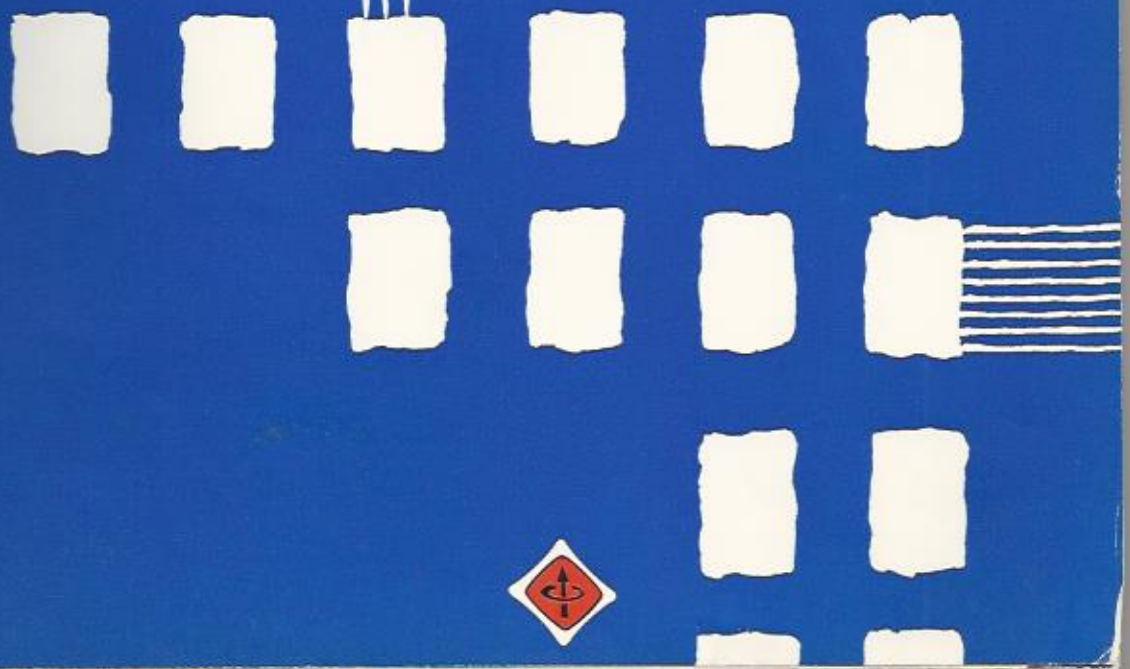

[37] A. R. Strube, "LSI for high-performance logic applications," presented at the Internat'l Electron Devices Meeting, October 1967.
[38] M. P. Lepselter, "Air-insulated beam-lead crossovers for integrated circuits," *Bell Sys. Tech. J.*, vol. 47, pp. 269–271, February 1968.
[39] C. D. Parker, "Reliability," in *Integrated Silicon Device Technology*, vol. 15, Research Triangle Institute, Research Triangle Park, N. C., Rept. AD 655082, May 1967.
[40] D. K. Lynn, C. S. Meyer, and D. J. Hamilton, *Analysis and Design of Integrated Circuits*. New York: McGraw-Hill, 1967, pp. 341–360.
[41] D. Kahng and S. M. Sze, "A floating gate and its application to memory devices," *Bell Sys. Tech. J.*, vol. 46, pp. 1288–1295, July–August 1967.
[42] H. A. R. Wegener, A. J. Lincoln, H. C. Pao, M. R. O'Connell, and R. E. Oleksiak, "The variable threshold transistor, a new electrically-alterable, nondestructive read-only storage device," presented at the Internat'l Electron Devices Meeting, October 1967.
[43] R. S. Dunn, "The case for bipolar semiconductor memories," *Fall Joint Computer Conf., AFIPS Proc.*, vol. 31, pp. 596–598, November 1967.
[44] S. Waaben, "High-speed plated-wire memory system," *IEEE Trans. Electronic Computers*, vol. EC-16, pp. 335–343, June 1967.
[45] R. J. Petschauer, "Magnetics—Still the best choice for computer main memory," *Fall Joint Computer Conf., AFIPS Proc.*, vol. 31, pp. 598–600, November 1967.
[46] E. W. Pugh, V. T. Shahan, and W. T. Siegle, "Device and array design for a 120-nanosecond magnetic film main memory," *IBM J.*, vol. 11, pp. 169–178, March 1967.
[47] Q. W. Simkins, "Planar magnetic film memories," *Fall Joint Computer Conf., AFIPS Proc.*, vol. 31, pp. 593–594, November 1967.
[48] T. J. Gilligan, "2½D high speed memory systems—Past, present, and future," *IEEE Trans. Electronic Computers*, vol. EC-15, pp. 475–485, August 1966.

Dynamic Scattering: A New Electrooptic Effect in Certain Classes of Nematic Liquid Crystals

GEORGE H. HEILMEIER, SENIOR MEMBER, IEEE, LOUIS A. ZANONI, AND LUCIAN A. BARTON

Abstract—**A new electrooptic effect in certain classes of nematic liquid crystals is presented. The effect has been termed "dynamic scattering" because scattering centers are produced in the transparent, anisotropic medium due to the disruptive effects of ions in transit. The ions can be produced by field assisted dissociation of neutral molecules and/or Schottky emission processes. The rise times of 1 to 5 ms and decay times of less than 30 ms, together with dc operating voltages in the 10 to 100 V range, make dynamic scattering seem attractive for such applications as alphanumeric indicators, and do not preclude its use in line-at-a-time matrix addressed, real-time displays. Reflective contrast ratios of better than 15 to 1 with efficiencies of 45 percent of the standard white have been demonstrated.**

Liquid Crystals—Nematic Phase

THE FIELD of liquid crystals has been the subject of reviews by Gray [1] and Brown and Shaw [2], hence a comprehensive review will not be attempted here. Nevertheless, some general information necessary to familiarize the reader with this rather exotic field will facilitate an understanding of the new effect and its possible applications.

The term "liquid crystals" is applied to substances whose rheological behavior is similar to that of fluids but whose optical behavior is similar to the crystalline state over a given temperature range. Liquid crystals are by no means rare. Approximately one out of every 200 organic compounds exhibits mesomorphic behavior, although the occurrence in inorganic substances is extremely uncommon. Both aliphatic and aromatic compounds can exist as liquid crystals.

Manuscript received January 16, 1968.
The authors are with RCA Laboratories, Princeton, N. J. 08540

The feature common to molecules exhibiting liquid crystallinity is a planar, rod-like structure. Three classes of mesomorphic behavior exist: smectic, cholesteric, and nematic. As evident in Fig. 1, each is characterized by a specific arrangement of molecules in the fluid. Cholesteric liquid crystals have been used as temperature and vapor indicators [3]. We shall restrict ourselves to a brief discussion of the nematic state which is the particular mesophase exhibiting our electrooptic effect.

The term "nematic" is derived from the Greek word meaning thread. This term describes the thread-like lines which can be seen in this class of liquid crystals under a microscope. The molecules of nematic liquid crystals are arranged with their long axes parallel but not in layer form as is the case with smectic liquid crystals (see Fig. 1). The molecules are free to slide past each other; nevertheless, they remain essentially parallel within a given region. Nematic materials can be aligned by both electric and magnetic fields. This alignment can be essentially complete [4] in contrast to the relatively weak alignment produced by high fields in conventional polar fluids (i.e., one part in 10^4) as predicted by Langevin theory ($\sim \mu E/kT$, μ=dipole moment, E=electric field). This follows from the cooperative behavior of the molecules in the nematic liquid crystal.

Probably the best known nematic substance and one whose rheological, optical, and electrical properties have been extensively explored is *p*-azoxyanisole. This material transforms from a crystalline solid into the nematic state at 116°C and becomes an isotropic liquid at 133°C.

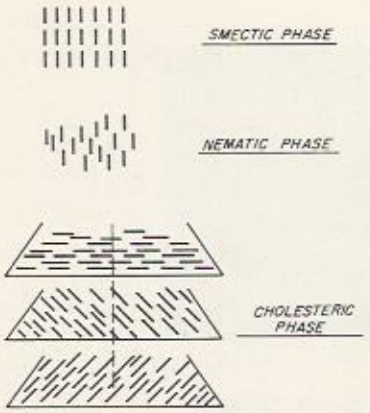

Fig. 1. Molecular alignment for various mesophase types.

Phenomenological Description of the Effect

The structure which we wish to consider is a sandwich cell consisting of a transparent front electrode (i.e., nesa-coated glass) and a specularly reflecting back electrode. This is seen in Fig. 2, cell I. The nematic material is sandwiched between these electrodes using teflon spacers of $\frac{1}{4}$ to 1 mil thickness. Capillary action is sufficient to hold the liquid between the plates for a variety of orientations. In general, some means for maintaining the temperature within the nematic range is required.

In its quiescent state with no field applied, the liquid crystal is essentially transparent. This means that if the specularly reflecting back electrode is faced into a black background, the cell appears black. When a dc field of the order of 5×10^3 V/cm (corresponding to 6 V for a $\frac{1}{2}$ mil thick sample) is applied, the liquid becomes turbulent and scatters light. We have designated this state as the *dynamic scattering mode* (*DSM*). In this state the cell appears white. Increasing the field results in increased brightness so that a gray scale is obtainable. Saturation of contrast ratio versus field occurs at about 5×10^4 V/cm. A typical result is shown in Fig. 3. Under dc conditions maximum contrast ratios in excess of 20 to 1 with maximum brightness of the order of 50 percent of $MgCo_3$ (the standard for white) have been obtained under conditions where the specular reflecting back electrode "looks" into a black background.

While we have discussed this effect phenomenologically as a reflective effect, the true operation is due to the scattering of light. It is characteristic of nonconducting scattering centers which are larger than 5 to 10 times the wavelength of the incident light that the scattered radiation is not a function of the incident wavelength [5]. Moreover, the bulk of the radiation is forward scattered rather than backscattered; thus, a specular reflecting back electrode is necessary to direct this radiation back through the scattering medium to subjectively maximize the effect.

Materials

The materials which have yielded the best performance in the dynamic scattering mode of operation are members of a class of organic compounds known as Schiff bases. These materials, when highly pure, are essentially transparent in the visible and have resistivities of 1 to 5×10^{10} $\Omega \cdot$cm and a dielectric constant of 3.5 at 90°C. We have found the compound APAPA (anisylidene para-aminophenylacetate), shown in Fig. 4, to be of particular interest in demonstrating the dynamic scattering mode [6]. Its nematic range is from 83°C to 100°C.

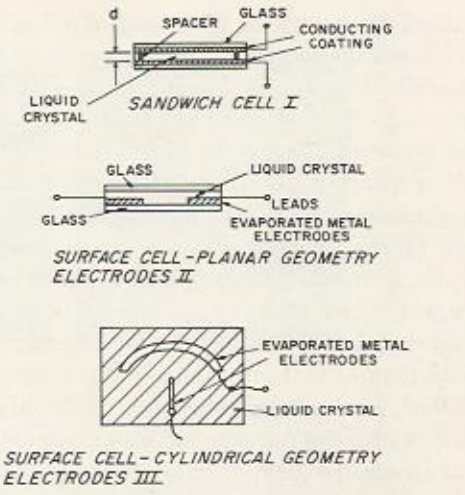

Fig. 2. Cell configurations.

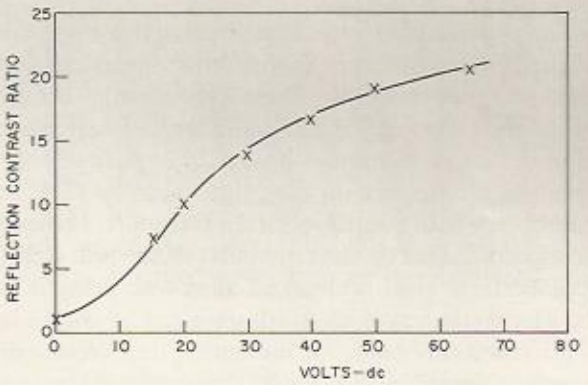

Fig. 3. Reflection contrast ratio versus voltage. Material: C_1-APAPA; cell thickness $\sim \frac{1}{2}$ mil.

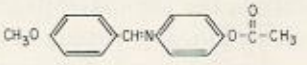

Fig. 4. Anisylidene-*p*-aminophenylacetate.

Driving Mechanism of the Dynamic Scattering Mode

The turbulence noted in the liquid crystal when subjected to fields above threshold requires that domain-like regions of neutral molecules be set in motion. Scattering is produced

by localized variations in the index of refraction. As we have discussed, these regions must be large compared to the wavelength of the incident radiation. Their nature will be explored more fully in another section.

There are several mechanisms by which an electric field can exert a force on a fluid: 1) electrostriction, 2) spatially varying dielectric constant, 3) dielectrophoresis, 4) electrophoresis, 5) electrohydrodynamic effects. Mechanisms 4) and 5) are somewhat related. To review briefly, electrostrictive forces arise from the change in dielectric constant produced by field induced density changes. Dielectrophoresis is defined as the motion of matter caused by polarization effects in a nonuniform field. Electrophoresis is the motion of a charged particle and its associated counterion cloud in an electric field. The counterions themselves are moving, on the average, in the opposite direction under the influence of the applied field. Since they are solvated, they tend to carry with them their associated solvent molecules, so that there is a net flow of solvent in a direction opposite to the motion of any given (solvated) central charge.

What we shall call electrohydrodynamic forces [7], [8] are those mechanical forces which are produced by essentially unipolar electrical conduction. When ions in a partly ionized medium move under the influence of an electric field, friction with the carrier medium transfers momentum to the latter. If only one sign of ion is present, the pressures created can be significant.

We have performed experiments using five basic sample configurations in an effort to determine the mechanism or mechanisms of the DSM. These experimental configurations are shown in Fig. 2. Cell I is similar to the arrangement used in the actual display with $6\mu < d < 25\ \mu$. In cells II and III both electrodes are on the same substrate. The liquid crystal covers both electrodes, and a transparent cover slide with spacers makes up the remainder of the cell. Cell IV is fabricated from glass tubing and filled with nematic materials. The metal screen electrodes are spaced 5 mm apart. and provisions are made for measuring the pressure difference across the cell with electric field applied.

In cell I, for thicknesses less than 25 μ, with one nesa-coated glass electrode and one metal electrode, the DSM is always greater at a given voltage when the metal electrode is negative. In addition, the current-voltage characteristic is not linear, as seen in Fig. 5. A threshold of 5 to 10 kV/cm for the DSM is generally found. Transient measurements, to be described more completely in a later section, were also made using this type of cell. When the cell was subjected to a voltage step, the current, in addition to exhibiting an initial displacement current transient, also possessed a later secondary peak similar to that found for transient space charge limited currents in solids (see Fig. 6) [9]. The time of occurrence of the secondary peak or "cusp" was inversely proportional to the applied voltage, as seen in Fig. 7. This secondary peak was not seen when one of the electrodes was made an ideal blocking contact by covering it with teflon. In addition, no optical effect was seen under these conditions. Unfortunately, measurements as a function of cell thickness were nonreproducible in a consistent manner due

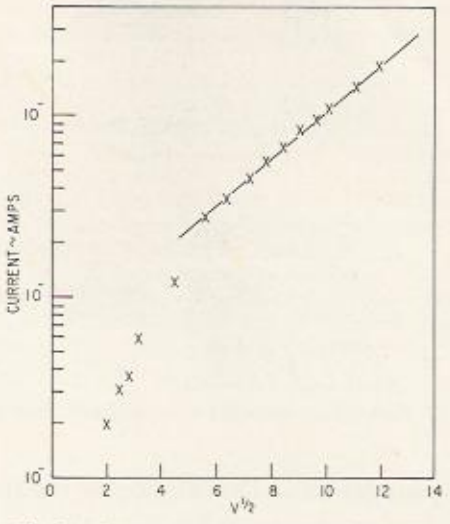

Fig. 5. Current versus voltage sandwich cell. Thickness $\sim \frac{1}{4}$ mil; T ~ 90°C.

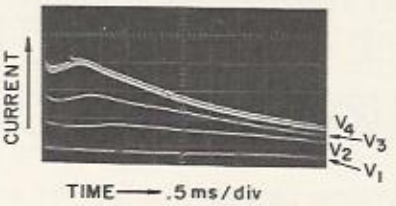

Fig. 6. Typical current transient.

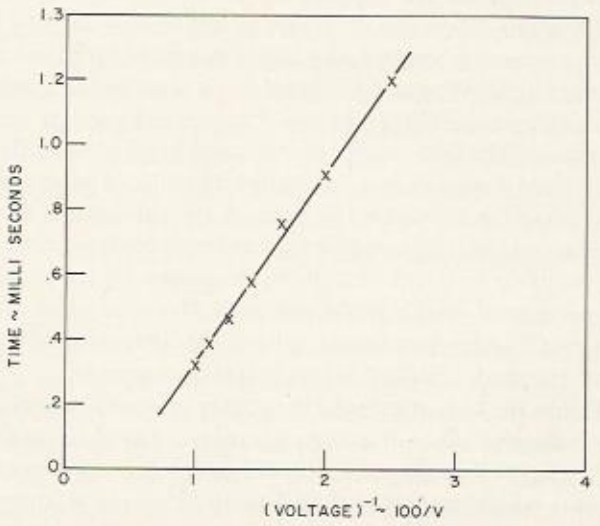

Fig. 7. Position of cusp (time) versus (voltage)$^{-1}$. Material: APAPA; electrode separation $\sim 12\ \mu$.

to the nature of the cell fabrication technique.

When cell III was viewed under the same conditions with crossed polarizers, an optical effect (i.e., change in transmitted light) was seen to initiate at the *negative* electrode and travel to the positive electrode. At threshold field the effect initiated nonuniformly at the negative electrode.

When cell III was viewed under the same conditions as above with the smaller-radius electrode negative, the optical effect initiated at the negative electrode for fields about the

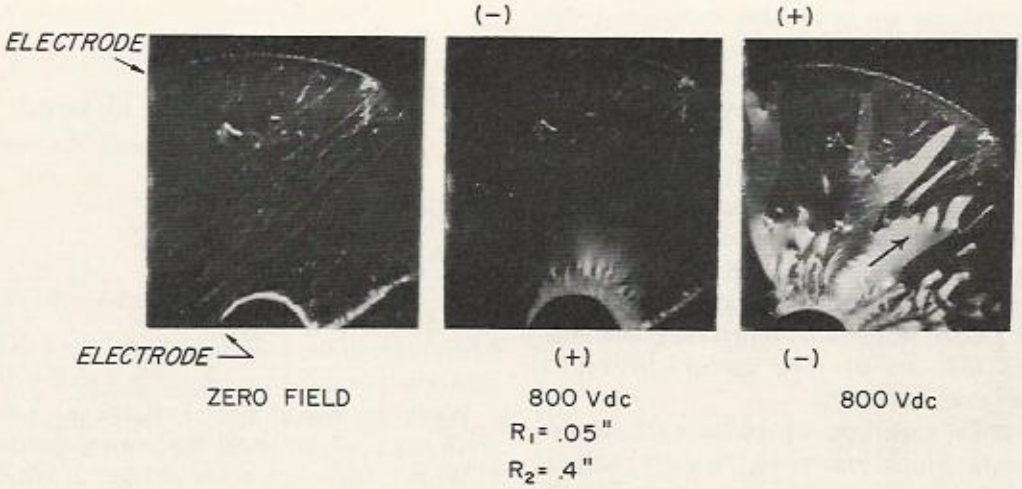

Fig. 8. Cylindrical electrode system—optical effects.

same as those observed for the sandwich cell. This optical effect at threshold also propagates to and terminates at the anode, as seen in Fig. 8. The propagation rate appeared to be nonuniform, slowing noticeably near the anode. In this geometry with the field at the small electrode equal to 5 to 10 kV/cm, that at the anode is much less and substantially *below* threshold.

In cell IV, although the electrode separation is orders of magnitude greater than that of cell I, turbulence in the liquid crystal initiates at roughly the same field strength. The appearance of an optical effect is accompanied by a rise in pressure at the anode. The difference in the height of the column at the anode and at the cathode as a function of field is shown in Fig. 9, along with the current.

Another cell similar to IV without the provisions for measuring pressure was also used. This cell had two solid metal electrodes separated by a metal screen electrode (see Fig. 2, cell V). It was found that the current was 10 to 15 percent higher when the screen electrode was positive and only one of the solid electrodes was used as a cathode, compared to the case with the polarities reversed. Optical effects were also noted in the field free region beyond the screen anode. When both solid electrodes were used as the cathode, the current to the screen anode in the center of the cell was not doubled as might be expected.

It is recognized that the widely different cell and electrode geometries and sizes may themselves help determine which of the several possible effects may be dominant in driving the DSM in a specific experiment. Nevertheless, if we choose to minimize this possibility and assume that there is experimental consistency independent of the geometry, we can summarize our data as follows: 1) The appearance of the optical effect initiates at the negative electrode. 2) It is accompanied by an increase in pressure at the anode and the deviation of the current-voltage characteristic from linear to a more rapid variation with voltage. 3) The magnitude of the optical effect at a given field is dependent on the nature of the negative electrode. 4) The optical effect which initiates at the cathode propagates to the anode, although the field in this region may be far below threshold for the effect.

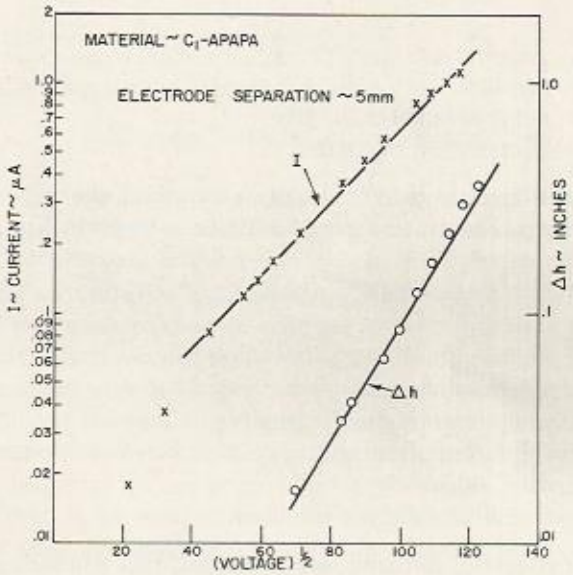

Fig. 9. Current and pressure versus voltage.

5) The experiments with cell V indicate that there is a definite relationship between electrical and optical effects and hydrodynamic effects. 6) Transient measurements indicate that the passage of current is necessary to produce the DSM.

Now let us critically examine these observations. Forces due to electrostriction and/or spatially varying dielectric constant cannot account for the pressure rise at the anode. In addition, these forces would not require current to be passed, which seems necessary for the DSM. Dielectrophoresis requires a nonuniform field. In our planar geometry this could only be produced by space charge. Nevertheless, the experiments with cylindrical geometry electrodes with the high field at the cathode saw the optical effect still propagate *from* cathode to anode, which is contrary to what would be predicted for dielectrophoresis. Other true field effects are also suspect when we note that the optical effect in the aforementioned case propagates through regions where the field is far below normal threshold for the effect. Thus, a model based on dielectrophoresis does not seem consistent with all the experimental data.

The experiments in one way or another seem to eliminate all possibilities except those based on charge transport as the mechanism for the DSM. Electrohydrodynamic effects require charge transport in the liquid crystal to be dominated by one sign of carrier. Positive ions are not felt to be the dominant carriers, since the pressure rise is at the anode, the optical effect initiates at the cathode, and the effect is somewhat sensitive to cathode material. The means of producing transport imbalance include preferential adsorption or accumulation of one type of ion at the walls of the container and/or electrode, mobility differences, and injection of electrons followed by their capture by neutral molecules (forming negative ions).

Fundamental to the experimental results is the requirement that the electrical force present on the space charge in the fluid must be balanced by a pressure gradient given by

$$\nabla p = \rho E \tag{1}$$

where

p = pressure
ρ = net space charge density
E = electric field strength.

Using Poisson's equation and integrating, the pressure difference between anode and cathode is given by

$$\Delta p = \tfrac{1}{2}\varepsilon_0\varepsilon(E^2_{\text{anode}} - E^2_{\text{cathode}}) = Tg\Delta h \tag{2}$$

where

T = density of fluid
g = acceleration due to gravity
Δh = difference in height of column between anode and cathode
ε = relative dielectric constant.

If the effects of diffusion are neglected, this equation can be written

$$\Delta p = L\sum_i J_i/\mu_i \tag{3}$$

where J_i represents the various contributing conduction processes, and L is the electrode spacing. If the dominant conduction mechanism is also the dominant contributor to the pressure generation, a plot of Δp versus V will have the same behavior as J versus V. If this is not the case, the behavior of the two plots will differ. Pressure and current-voltage data are shown in Fig. 9. Note that the slope of the ln (pressure) versus $V^{1/2}$ is greater than ln (I) versus $V^{1/2}$, indicating that we are probably dealing with separate mechanisms in this case. Pickard [10] has examined in detail the variation of pressure with the uniform V/L in conventional liquids in terms of a parameter η which reflects changing space charge conditions. Our data fit the case where η is increasing monotonically to one as the voltage is increased.

As an example of how subtle field differences between anode and cathode in the presence of larger average fields can lead to the observed pressure differences, consider the case shown in Fig. 9.

$$\Delta p = \tfrac{1}{2}\varepsilon_0\varepsilon(E^2_{\text{anode}} - E^2_{\text{cathode}}) = Tg\Delta h \tag{4}$$

where

T = density $\sim 1.3 \times 10^3$ kg/m^3
$g \doteq 9.8$ m/s^2
$\varepsilon_0\varepsilon \sim 36 \times 10^{-12}$ F/m
$\Delta h|_{V=10\text{kV}} \sim 2.2 \times 10^{-3}$ m.

Hence,

$$(E^2_{\text{anode}} - E^2_{\text{cathode}}) \sim 1.5 \times 10^{12}\ (\text{V/m})^2. \tag{5}$$

The square of the average field for the 4 to 5 mm electrode separation in the pressure cell is 4 to 6×10^{12} (V/m)^2.

While the importance of charge in producing dynamic scattering has been established, two major questions remain. 1) What is the origin of the charge? 2) What are the details of the process which produces scattering centers in the liquid? These questions are the subject of the following sections of this paper.

Conduction Studies and Their Relevance to Dynamic Scattering

In the previous section it was established that a relationship does exist between dynamic scattering and the production of a pressure difference between anode and cathode when field is applied. Dc current-voltage data for the pressure cell and sandwich cell (see Fig. 2), where the electrode spacings are 15 cm and 6×10^{-4} cm, respectively, are shown in Figs. 9 and 5, respectively. Note that the data give an excellent fit to an $I \propto \exp(V^{1/2})$ law. The slope has a value of 2.48×10^{-3} (MKS) for the sandwich cell and 2.7×10^{-3}(MKS) for the pressure cell. These values do not compare favorably to the theoretical value of

$$e^{3/2}/2kT(\pi\varepsilon\varepsilon_0)^{1/2} \sim 0.88 \times 10^{-3}\ (\text{MKS})$$

for Schottky emission which has the same functional dependence [11]. Measurements could not be made over a significantly wide temperature range to check the temperature dependence of the slope.

Experiments in the sandwich cell geometry with evaporated aluminum, nickel, cobalt, platinum, and chromium cathodes revealed a difference in current of no more than a factor of ten for fields up to 10^5 V/cm and no consistent dependence on cathode work function. The thickness dependence of the current is shown in Fig. 10. Note that the current increases linearly with increasing sample thickness. This is, indeed, contrary to ohmic and Schottky emission behavior where a decrease is expected.

As a final check, a cell with an electrode geometry of a point and a plane was fabricated. No significant variation in current was found at fixed voltage when the polarity of the voltage on the cell was reverse. Schottky emission is dependent on the field at the cathode. In the case of the point cathode, conditions favoring emission certainly existed, yet no variation in current was observed.

We can summarize the experimental conductivity studies by noting that 1) $I \propto \exp kV^{1/2}$ where the experimental value for k is a factor of 2 to 3 times larger than that pre-

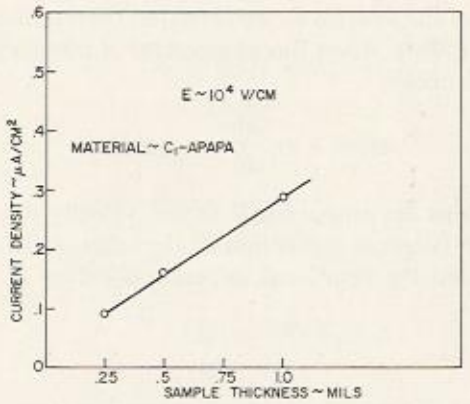

Fig. 10. Current density versus sample thickness for constant applied field.

dicted by Schottky emission; 2) little or no dependence was found on electrode work function or field configuration; and 3) current *increased* with increasing electrode separation.

The data are consistent with a model based on field assisted molecular dissociation of the liquid or impurities therein. In general, if we assume essentially no space charge, the current is given by

$$J = eE(n\mu_n + p\mu_p) \tag{6}$$

and

$$\nabla \cdot J_n = e\mu_n E \frac{dn}{dx} = cD(E) - \gamma np \tag{7}$$

where

E = average electric field
μ_n, μ_p = negative and positive ion mobilities, respectively
n, p = negative and positive ion densities, respectively
$D(E)$ = field assisted dissociation constant
γ = recombination constant
c = constant.

If, in the spirit of the semiquantitative nature of this analysis, we assume that

E = constant (no space charge)
$n = p$
$\mu_n = \mu_p$
$\gamma = 0$ (direct recombination is small)
$n = 0$ (at cathode),

then (7) can be integrated simply to yield

$$n = \frac{cD(E)}{\mu Ee} L$$

where L = electrode spacing. Since we have assumed that $n \sim p$ and $\mu_n \sim \mu_p$,

$$J = 2cD(E)L. \tag{8}$$

It remains to develop a simple expression for the field assisted dissociation constant.

In the absence of field, this has the general form

$$D(0) = D_0 \exp(-U_0/kT) \tag{9}$$

where U_0 = dissociation energy in the absence of field. Using the same general approach of simplified derivations of the Schottky emission equation [11], the dissociation energy is given by the integrated sum of the electrostatic forces

$$U(E) = \int_0^{x_c} \frac{-e\,dx}{4\pi\varepsilon\varepsilon_0 x^2} - \int_0^{x_c} eE\,dx$$

$$= U_0 - \frac{e^2}{4\pi\varepsilon\varepsilon_0 x_c} - eEx_c. \tag{10}$$

Now when $x = x_c$, the net force is zero; hence,

$$x_c = \left(\frac{e}{4\pi\varepsilon\varepsilon_0 E}\right)^{1/2} \tag{11}$$

and the dissociation energy becomes

$$U = U_0 - 2e^{3/2}\left(\frac{E}{4\pi\varepsilon\varepsilon_0}\right)^{1/2}. \tag{12}$$

Substitution of (9) and (12) in (8) yields the current-voltage relationship for the dissociation model

$$J = 2cLD_0 \exp\{-U_0 + 2e^{3/2}(E/4\pi\varepsilon\varepsilon_0)^{1/2}\}/kT. \tag{13}$$

Note that the slope of a $J \propto \exp V^{1/2}$ plot is twice that of the Schottky emission model, and an *increase* in current with electrode separation is predicted. In addition, no dependence on electrode work function is indicated.

While possessing some similarities with Schottky emission, the field assisted dissociation model offers much better agreement with our experimental data and seems to be the dominant conduction process. This is not to say that it is the only active conduction mechanism in our experiments. The initiation of an optical effect at the negative electrode followed by its propagation to the anode could be due to a field nonuniformity or an emission process. Thus, while field assisted dissociation may dominate the conduction process, it is still possible that an emission process which is enhanced by high fields at the cathode may be a factor in the dynamic scattering. This emission process would seem to have much in common with Schottky emission, and indeed I-V data in agreement with this mechanism were found in *one* sample. This finding leads us to suspect that the dissociating species is an impurity molecule.

A Model for Dynamic Scattering Based on Shear Induced Alignment by Ions in Transit

Previous experiments have emphasized the importance of ions in transit in producing dynamic scattering in certain classes of nematic liquid crystals. In further work it was found that little or no dynamic scattering is present in nematic systems whose molecular dipole moment lies along the molecular axis, although resistivities may be quite comparable to those for which the effect is observed in the APAPA family. Such a material is *p-n* ethoxybenzylidene-*p'*-aminobenzonitrile (PEBAB), shown in Fig. 11. We have also found that dynamic scattering can be produced without an electric field by moving one electrode along the other in the sandwich cell geometry, thus subjecting the liquid

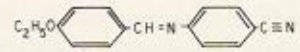

Fig. 11. *p-n*-ethoxybenzylidene-*p'*-aminobenzonitrile.

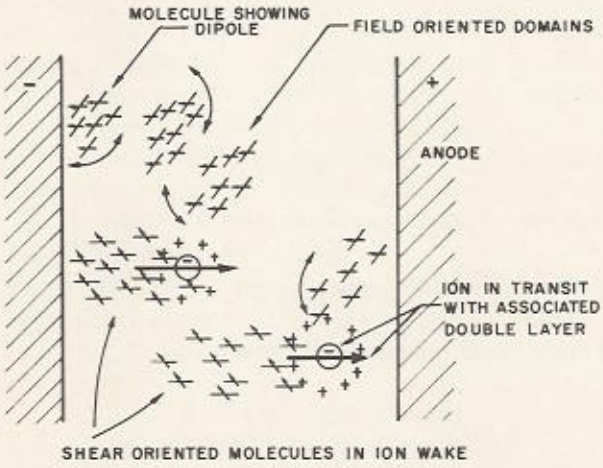

Fig. 12. Molecular model of the dynamic scattering mode.

crystal to a mechanical shear. The shear in this case is roughly 1000 s^{-1}.

In an effort to explain these varied experimental observations, we wish to propose a model based on the alignment of swarms due to the shear induced in the liquid crystal by the ions in transit. This alignment, which is dynamic in nature, tends to align the *molecular axis* along the direction of ion transit (see Fig. 12). The electric field, on the other hand, tends to align the dipole moment along the direction of the applied field. In molecules where the dipole moment does not lie along the molecular axis, each of these two forces tends to produce a different alignment, and since the swarms are highly birefringent, the conditions for light scattering exist between the differently oriented regions. In the case where the dipole moment and molecular axis lie in the *same* direction, the field induced alignment and the shear induced alignment are in the same direction, and scattering centers are not dramatically evident.

Consider a rod-shaped domain in a shear field $g = dv_x/dy$. The major axis of the domain lies at an angle θ with respect to the x-axis. If the swarm axis is not aligned in the direction of flow, the ends of the swarm will experience a transverse component of velocity:

$$v_t = 1/2Lg \sin^2 \theta \tag{14}$$

where L = swarm length. Neglecting inertial effects, the angular velocity of the swarm axis is simply

$$\dot{\theta} = g \sin^2 \theta. \tag{15}$$

The probability Φ of finding a swarm in any given orientation will be inversely proportional to the rotational speed; hence,

$$\Phi\dot{\theta} = \text{constant}. \tag{16}$$

The rotational thermal motion of the swarms tends to counteract the hydrodynamic orientation effects. This thermal component of the motion gives rise to an orientational diffusion of the swarms in the direction corresponding to a decrease of $\Phi(\theta)$. When this component of motion is added to (16), we obtain

$$\Phi(\theta)\dot{\theta} - D_r \frac{d\Phi}{d\theta} = \text{constant}. \tag{17}$$

Since $\dot{\theta}$ must be proportional to the velocity gradient or shear g, Φ becomes a function of the ratio of the velocity gradient and the rotational diffusion constant D_r. Hence,

$$\Phi = f(\alpha)$$

$$\alpha = g/D_r.$$

Equation (17) can be solved by series techniques. Two special cases are of interest.

Case 1

Let

$$\alpha < 1$$

$$\Phi = 1 + \sum_1^\infty \alpha^m g_m(\theta).$$

Substituting in (17) and equating coefficients yields

$$\Phi = 1 + \frac{\alpha}{4} \sin 2\theta + \cdots. \tag{18}$$

The alignment tendency is weak but tends to have a maximum at $\theta = \pi/4$.

Case 2

Let

$$\alpha \gg 1$$

$$\Phi = \sum_1^\infty \alpha^{-n} g_n(\theta).$$

Again substituting in (17) and equating coefficients, we obtain

$$\Phi = \frac{\text{constant}}{\alpha \sin^2 \theta} + \cdots. \tag{19}$$

In this case the swarm axes tend to align along the flow axis, and the distribution function is sharpened and peaked, compared to Case 1, about $\theta = 0$.

Previous experiments on dynamic scattering have revealed the importance of ions in transit in producing the effect. We now consider some of the consequences of this motion. An ion in solution tends to move with its own characteristic velocity v_0 which is independent of other ions in solution. However, the ion atmosphere, being of opposite sign, will tend to move in the opposite direction. This introduces a retarding effect on this central ion. Each element in the ion atmosphere is acted upon by a force per volume which is the product of the space charge density and the field. The space charge is given by

$$\rho = \frac{e\lambda^2 \exp(\lambda a - \lambda r)}{4\pi(1 + \lambda a)r} \tag{20}$$

where

$$a = \text{ion radius}$$

$$(\lambda)^{-1} = \text{Debye length.}$$

Hence,

$$\text{force/volume} = \rho E$$

and

$$\text{force} = \int 4\pi r^2 \rho E \, dr.$$

This force produces a drag on the central ion corresponding to a velocity v_d. If we assume that the ions are essentially spherical and that the Stokes law holds,

$$v_d = \frac{F}{6\pi\eta r}$$

$$dv_d = \frac{dF}{6\pi\eta r} = -\frac{E\lambda^2 e \exp(\lambda a - \lambda r)}{6\pi\eta(1 + \lambda a)} dr \tag{21}$$

where η = coefficient of viscosity. Integrating from the closest distance of approach, a, to infinity yields

$$v_d = -\frac{Ee\lambda}{6\pi\eta(1 + \lambda a)}. \tag{22}$$

For dilute solutions $\lambda a \ll 1$ (low conductivity)

$$v_d = -\frac{Ee\lambda}{6\pi\eta}.$$

The net velocity of the central ion is

$$v = v_0 - |v_d| = \frac{eE}{6\pi\eta}\left(\frac{1}{a} - \frac{1}{\delta}\right) = \frac{eE}{6\pi\eta}\left\{\frac{\delta - a}{a\delta}\right\} \tag{23}$$

where $\delta = \lambda^{-1}$ = Debye length. The motion of the central ion and the counterion cloud tends to shear the fluid surrounding the ion. Solely for the sake of a rough quantitative estimate, we assume that the shear is given by

$$g \sim \frac{v_0 - |v_d|}{\delta}. \tag{24}$$

In our materials the Debye length is of the same order as the average distance between ions.

In nematic liquid crystals we have found that the ion mobility is $\sim 10^{-4}$ cm^2/V·s. For the fields of roughly 10^4 V/cm which are necessary for dynamic scattering, this corresponds to $\Delta v \sim 1$ cm/s. Debye lengths for the materials which are of interest are usually $\sim 0.5\ \mu$. Hence,

$$g \sim 2 \times 10^4 \text{ s}^{-1}.$$

As we have previously shown, the orientation of swarms in a shear flow is governed by the parameter α.

$$\alpha = g/D_r = \text{shear/rotary diffusion coefficient.}$$

The rotary diffusion can be estimated if we assume that the axial ratio of the swarm is approximately unity (spherical). According to Morawetz [12],

$$D_r = kT/8\pi\eta R^3 \tag{25}$$

where

R = swarm radius $\sim 0.1\ \mu$

η = coefficient of viscosity $\sim 3 \times 10^{-3}$ (MKS).

For our case

$$D_r \sim 50.$$

Thus,

$$\alpha = g/D_r \sim 400.$$

Our previous calculations indicated that appreciable alignment along the direction of flow was obtained for $\alpha \gg 1$; hence, it appears that the swarms are capable of being aligned by the shear induced by ions in transit. When we pass to the isotropic state the molecules are no longer associated, and the size of the orienting species is that of the individual molecule ($R \sim 20$ Å). Hence,

$$D_r \sim 6.6 \times 10^6 \text{ s}^{-1}$$

and

$$\alpha \sim 3.3 \times 10^{-3}.$$

This value of α is too small to produce alignment and hence no dynamic scattering is observed in the isotropic state.

Some of the assumptions made in the course of this crude analysis are open to question, i.e., 1) swarm orients as a rigid body, 2) the simplified Stokes model of viscous friction, 3) the spherical shape used in estimating D_r, and 4) the use of the Debye length in calculating the shear. However, these calculations serve only to suggest the plausibility of a hydrodynamic orientation model for dynamic scattering and do not purport to establish it unequivocally. It is to be noted that a circulatory force on the liquid crystal which could generate an apparent turbulence can be predicted from (1) provided

$$\vec{\nabla} \times \vec{F} = \vec{\nabla} \times \rho\vec{E} = \vec{\nabla}\rho \times \vec{E} \neq 0.$$

Thus, a space charge gradient in a direction which is not parallel to the applied field is required. That such a gradient could exist in a fluid exhibiting optical and electrical anisotropy does not seem too remote.

Transient Behavior

Using the sandwich cell configuration, the response of the liquid crystal to a voltage step function was observed. The optical response was recorded using a 931A photomultiplier and oscillosope. Rise times of the order of 1 to 5 ms are possible with dc voltages in the 50 to 100 V range corresponding to fields in the vicinity of 10^4 V/cm. Both the rise and decay times are a function of temperature and sample thickness. While our data are limited to a relatively narrow range, behavior consistent with the following relationships has been found for APAPA:

$$\tau_{\text{rise}} \propto I^{-1}$$

and also

$$\tau_{decay} \propto \rho^{1/2} L^2$$

where

τ_{rise} = rise time
τ_{decay} = decay time
I = current
L = sample thickness
ρ = resistivity.

In view of the crucial role which ion transport plays in the DSM, it is not surprising that the rise time for the effect should be related to the number of ions and their velocity or, as we have seen, the current. Note that the decay time (defined as the time required to go from 90 percent to 10 percent of the initial level) seems to be proportional to the square of the sample thickness and the square root of the resistivity. The shape of the decay curve could not be accurately measured over more than an order of magnitude; nevertheless, it did *not* fit an $\exp k/t$ or $\ln(kt)$ type of behavior. This would seem to eliminate models based on classical diffusion and mechanisms in which the rate is determined by past events. A much better fit to the decay curve was obtained using a $(1-kt^{1/2})$ law suggested by Williams [13].

Using the hydrodynamic model presented in the previous section, the relaxation of dynamic scattering would seem to be closely related to a molecular reorientation process. Williams [13] has suggested that reorientation may initiate at the surface and propagate at a diffusion controlled rate. There is ample evidence for the importance of surface effects in the orientation and electrical behavior of nematic liquid crystals [14]. Williams assumes that the scattering intensity is proportional to the sample thickness. When the field is removed the scattered light takes the following form:

$$I_s(t) = \beta[L - 2x(t)] \tag{26}$$

where

L = sample thickness
x = distance from the sample wall.

This model is shown schematically in Fig. 13. In the simplest diffusion model (diffusion rate independent of the particular wall)

$$x(t) = D^{1/2} t^{1/2}. \tag{27}$$

Thus,

$$I_s(t) = I_0\left(1 - \frac{2D^{1/2}t^{1/2}}{L}\right) \tag{28}$$

which can be functionally fitted to our decay transients. Using our previous definition of decay time $(0.9I_0 - 0.1I_0)$

$$\tau = 0.8L^2/4D. \tag{29}$$

This model agrees with the experimentally determined thickness dependence.

It is also possible to infer the resistivity dependence from the Einstein relation for the diffusion coefficient by a somewhat circuitous route. The diffusion coefficient is assumed to be proportional to a mobility which is, in turn, inversely proportional to the effective radius and viscosity of the diffusing species. This behavior of the mobility[1] follows from the Stokes model for viscous friction. If it is further assumed that the effective radius is a function of the Debye length ($r \propto l_{Debye} \propto \rho^{1/2}$), an inverse square root dependence of the diffusion coefficient on resistivity follows directly.

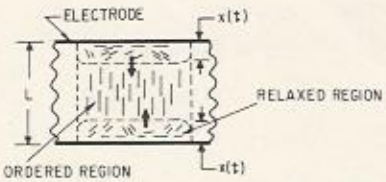

Fig. 13. Simplified model of the relaxation process.

Equation (29) can be directly checked with experiment. The value for the decay time of a 1/2 mil thick cell at 90°C is 30 ms. Using (29), this value implies a diffusion coefficient of 10^{-5} cm^2/s. On the basis of an Einstein model, the value of mobility should be

$$\mu = De/kT \approx 4.8 \times 10^{-4} \text{ cm}^2/\text{V}\cdot\text{s}.$$

As previously noted, a cusp was observed in the current transient (Fig. 6) which possessed much of the character of the familiar space charge limited current transient in solids [9]. If the transient is treated in this manner, one can calculate the mobility from the position of the cusp (Fig. 7). For our materials this value is approximately 0.3×10^{-4} cm^2/V·s, which is a typical value for ions in solution. Thus, the agreement between theory and experiment seems reasonably good in view of our crude model.

There are, however, certain inconsistencies in our attempt to relate the diffusion coefficient to the resistivity through the Debye length. According to the Stokes model for the ion mobility, one calculates (using the macroscopic viscosity) an effective radius in the 10 to 100 Å range for the mobilities which we have inferred from our data, while the Debye length is of the order of 0.1 to 0.5 μ. One can speculate on whether it is valid to use the experimental macroscopic viscosity in computing the mobility. Perhaps the motion is determined by a much smaller microscopic viscosity. There are dramatic reports in the literature in which the experimental mobility remained essentially constant while the macroscopic viscosity changed by orders of magnitude [15]. It is evident that more work must be done in this area if we are to understand the detailed effects of the microscopic viscosity on the mobility and, hence, the dependence of decay time on resistivity.

Evaluation of a Static Liquid Crystal Display Based on Dynamic Scattering

It is of interest to subjectively evaluate images produced by dynamic scattering. Using the sandwich cell geometry, the image was defined on the transparent electrode by a

[1] Mobility is inversely proportional to the product of effective radius and effective viscosity.

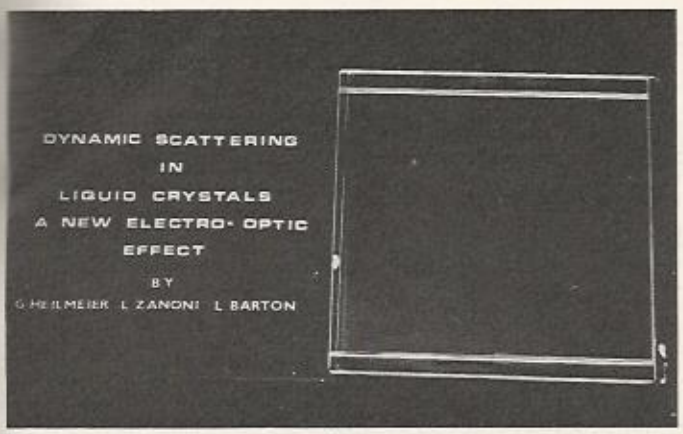

(a) Left: lettered card. Right: liquid crystal panel ($3\frac{1}{2}$ by 4 inches). $V=0$.

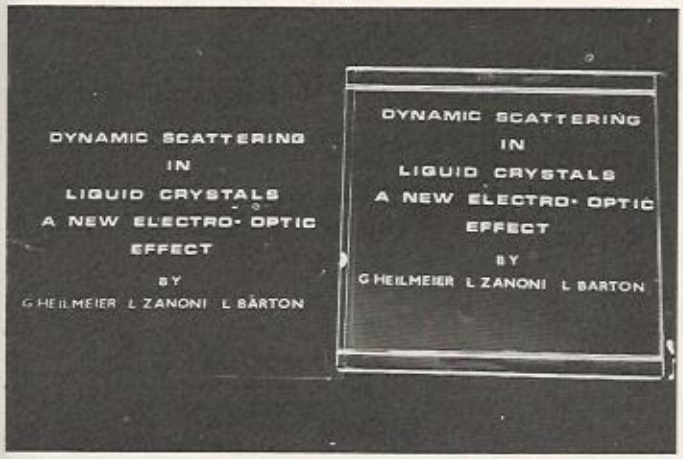

(b) $V=45$ V dc.

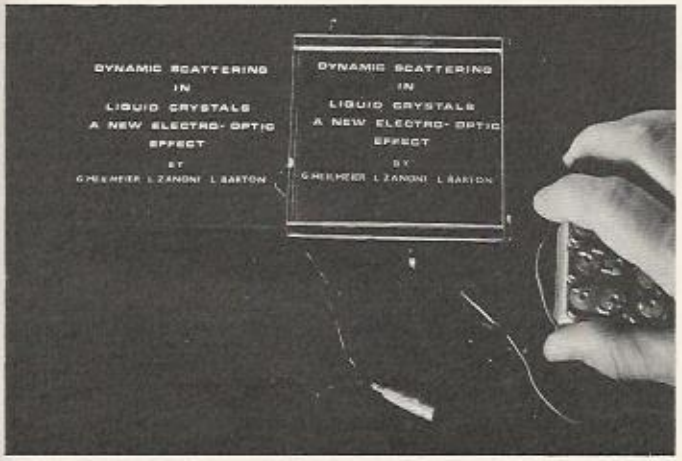

(c)

Fig. 14. Static image produced by dynamic scattering—qualitative evaluation.

transparent photoresist process. The photoresist is a much better dielectric than the liquid crystal; hence, field appeared across the liquid only in the regions from which the photoresist had been removed. Fig. 14 shows the quality of the image formed by the liquid crystal display compared to that of a printed page. The liquid crystal panel was roughly $3\frac{1}{2}$ by 4 inches, and the excitation was 45 V dc. The maximum contrast ratio on this panel was better than 20 to 1, and the areas of maximum brightness were 40 percent of the standard white ($MgCO_3$).

Dynamic Scattering and Transmitted Light

While this paper has dealt almost exclusively with the reflective mode of operation, the effects can also be observed in transmitted light. In this case, both electrodes in the sandwich cell geometry are transparent. With no field applied, light is transmitted by the cell. In its excited state the material scatters the incident light, thus reducing the amount of transmitted light. On-to-off ratios in excess of 20 to 1 have been obtained in this scheme.

Conclusions

A new reflective effect in certain classes of nematic liquid crystals has been discovered. The effect has been related to the disruptive effects of ions in transit through the aligned nematic medium which results in the formation of localized scattering centers. The ions can be produced by field assisted dissociation of neutral molecules and/or Schottky emission processes. The rise times of 1 to 5 ms and decay times of less than 30 ms, together with dc operating voltages in the 10 to 100 V range, make *dynamic scattering* seem attractive for such applications as alphanumeric indicators and do not preclude its use in line-at-a-time matrix addressed, real-time displays. Reflective contrast ratios of better than 15 to 1 with efficiencies of 45 percent of the standard white have been demonstrated.

Acknowledgment

The authors wish to thank J. Goldmacher and J. Castellano, who conducted the materials research connected with this project; J. Van Raalte, B. J. Lechner, D. Kleitman, and W. Moles, who provided support and insight into many problems relating to practical display applications; and Dr. R. Williams, who contributed many helpful discussions and insights into the field of liquid crystals.

References

[1] G. W. Gray, *Molecular Structure and Properties of Liquid Crystals*. London: Academic Press, 1962.
[2] G. H. Brown and W. G. Shaw, *Chem. Rev.*, vol. 57, p. 1049, 1957.
[3] J. L. Fergason, *Sci. Am.*, vol. 211, p. 77, 1964.
[4] R. Williams and G. H. Heilmeier, *J. Chem. Phys.*, vol. 44, p. 638, 1966.
[5] H. van de Hulst, *Light Scattering by Small Particles*. New York: Wiley, 1957.
[6] G. Hansen, unpublished dissertation, Halle, Germany, 1907.
[7] A. P. Chattock, *Phil. Mag.*, vol. 48, p. 401, 1899.
[8] O. Stuetzer, *J. Appl. Phys.*, vol. 30, p. 984, 1959.
[9] A. Many *et al.*, *J. Phys. Chem. Solids*, vol. 22) p. 285, 1961; also P. Mark and W. Helfrich, *Z. Phys.*, vol. 166, p. 370, 1962.
[10] W. F. Pickard, *J. Appl. Phys.*, vol. 34, p. 246, 1963.
[11] See, for example, A. Van der Ziel, *Solid State Physical Electronics*. Englewood Cliffs, N. J.: Prentice Hall, 1957.
[12] H. Morawetz, *Macromolecules in Solution*. New York: Interscience, 1965.
[13] R. Williams, private communication.
[14] See, for example, O. Pellet and P. Chatelain, *Bull. Soc. Franc. Mineral.*, vol. 73, p. 154, 1950; R. Williams, *J. Chem. Phys.*, vol. 39, p. 384, 1965; and R. Williams and G. H. Heilmeier, *J. Chem. Phys.*, vol. 44, p. 638, 1966.
[15] R. Taft and L. E. Malm, *J. Phys. Chem.*, vol. 43, p. 499, 1939.